ACS Macro Letters

Letter

Cite This: ACS Macro Lett. 2019, 8, 1413−1418

pubs.acs.org/macroletters

Thermal Degradation of Polystyrene under Extreme Nanoconfinement

Haonan Wang,[†] Yiwei Qiang,[‡] Ahmad Arabi Shamsabadi,[†] Prantik Mazumder,[§] Kevin T. Turner,[∥] Daeyeon Lee,[⊥] and Zahra Fakhraai*,[†]

[†]Department of Chemistry, University of Pennsylvania, Philadelphia, Pennsylvania 19104, United States

[‡]Department of Materials Science and Engineering, University of Pennsylvania, Philadelphia, Pennsylvania 19104, United States

[§]Corning Research and Development Corporation, Corning, New York 14830, United States

[∥]Department of Mechanical Engineering and Applied Mechanics, University of Pennsylvania, Philadelphia, Pennsylvania 19104, United States

[⊥]Department of Chemical and Biomolecular Engineering, University of Pennsylvania, Philadelphia, Pennsylvania 19104, United States

Supporting Information

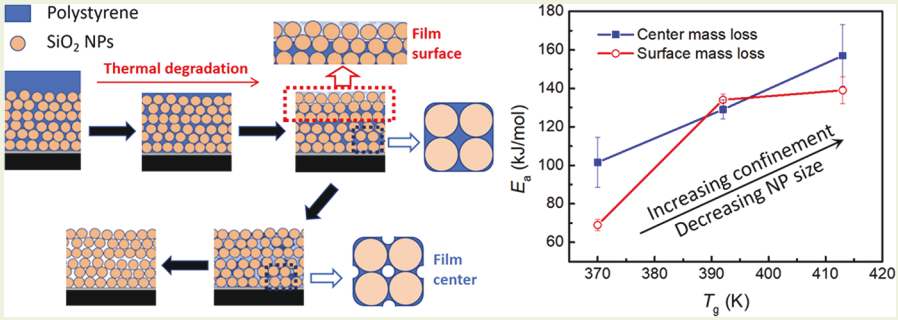

ABSTRACT: Extreme nanoconfinement has been shown to significantly affect the properties of materials. Here we demonstrate that extreme nanoconfinement can significantly improve the thermal stability of polystyrene (PS) and reduce its flammability. Capillary rise infiltration (CaRI) is used to infiltrate PS into films of randomly packed silica nanoparticles (NPs) to produce highly confined states. We demonstrate that as the NP size is decreased, increasing the degree of confinement, the isothermal degradation time is dramatically increased, by up to a factor of 30 at 543 K for PS confined in ∼3 nm pores. The activation energy of PS degradation is also increased, by 50 kJ/mol in the most confined state (∼3 nm pores). We demonstrate that the degradation proceeds through the film surface and from the center of large holes toward NP surfaces, indirect evidence that the process is diffusion limited. The surface-driven process dramatically reduces char formation even in large NP packings that show no significant changes in their dynamics and glass transition temperature (T_g) compared to the bulk.

Material properties deviate from bulk significantly when confined at the nanometer length scale. For polymeric materials, the reduction in the size and interfacial effects such as enhanced free surface dynamics[1,2] can significantly modify the physical aging rate,[3−7] viscosity,[8−10] and glass transition temperature (T_g).[1,11−16] Confinement and interfacial effects can also significantly influence chemical reactions at the nanometer length scale.[17−24] Unlike polymerization reactions, which have been extensively studied in confinement, little attention has been paid to polymer degradation reactions under extreme nanoconfinement. Understanding degradation under nanoconfinement is important for various applications, such as designing thermally stable and photostable coatings and organic electronics. Changing reaction pathways in confinement can also modify the reaction products and change the flammability of the confined polymer.

Degradation of polymers, in particular polystyrene (PS), in polymer nanocomposites (PNCs), can provide some insight into the degradation under extreme confinement. PNCs made with PS and clay show enhanced thermal stability at low nanoparticle (NP) loadings (between 0.75% and 18%).[25−30] The enhanced stability is believed to be due to the decrease in chain mobility and char promotion of clay, which act as mass transport barriers for the volatile products.[25] The existence of an optimal loading is because of NP aggregation at high loadings that changes the structure from nanocomposite to microcomposite. The enhancement of thermal stability of PS/SiO_2 nanocomposites is less significant, probably due to SiO_2's lack of catalytic ability as a char promoter.[26,28] In general,

Received: August 19, 2019
Accepted: October 3, 2019
Published: October 8, 2019

DOI: 10.1021/acsmacrolett.9b00649
ACS Macro Lett. 2019, 8, 1413−1418

PNCs made by conventional mixing methods have low loadings and poor control of NP dispersion.

Highly confined polymers with exceptionally high NP loadings can be achieved by capillary rise infiltration (CaRI).[31] In CaRI, polymers are infiltrated into the pores of a film of randomly packed NPs by annealing the system above the polymers' T_g. Due to the ultrahigh loading (~63% volume fraction for randomly packed NPs), uniform dispersion of NPs, and rigidity of the NP film, CaRI is a good model system to study the effect of extreme nanoconfinement on polymer properties. We have recently demonstrated that in CaRI viscosity[9,10] and T_g[16] are dramatically increased.

In this study, CaRI films made with unentangled PS and SiO_2 NPs are used to investigate the thermal degradation of highly confined polymers in ambient conditions. We demonstrate that the thermal degradation is significantly suppressed, and the activation energy for degradation is increased with decreasing pore size. The effect strongly correlates with the increased T_g, which is correlated with the loss of degrees of freedom of the segmental motion and is thus entropic in origin.[16]

CaRI films were prepared using the previously reported method,[16] as detailed in the Supporting Information (SI). Figure 1 schematically shows the steps used for the preparation

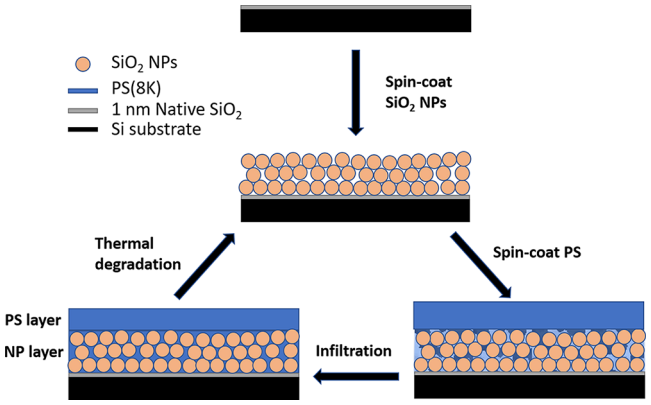

Figure 1. Schematic representation of the sample preparation and isothermal degradation measurements of PS/SiO_2 CaRI samples.

of PS (8 kg/mol)/SiO_2 CaRI samples and the measurements of the thermal degradation. Spectroscopic ellipsometry (SE) was used to determine the thickness and indices of refraction of each of the NP and PS layers (more details in the SI). Due to its rigid structure, the thickness of the NP layer does not change as the degradation proceeds.[16] As such, the degree of PS degradation inside the NP layer was evaluated based on the layer's index of refraction, which has a linear relationship with the volume fraction of PS.[32] To ensure that the NP layer was fully filled before the beginning of the experiments, an excess amount of PS was used, which resulted in a pure top PS layer, with a thickness less than 30 nm. The degradation of the top PS layer was monitored by changes in its thickness.

Figure 2a shows a typical measurement of the isothermal degradation of a PS (8K)/SiO_2 (100 nm) CaRI sample at 543 K. Here 8K is the molecular weight of PS in kg/mol, and 100 nm is the diameter of the NPs used. The plots show the degradation of the top PS layer (blue), which precedes the degradation of the confined PS inside the NP layer (black). Before the top PS layer is fully degraded (h_{PS} = 0 nm set as t = 0 s), the index of refraction of the NP layer stays constant,

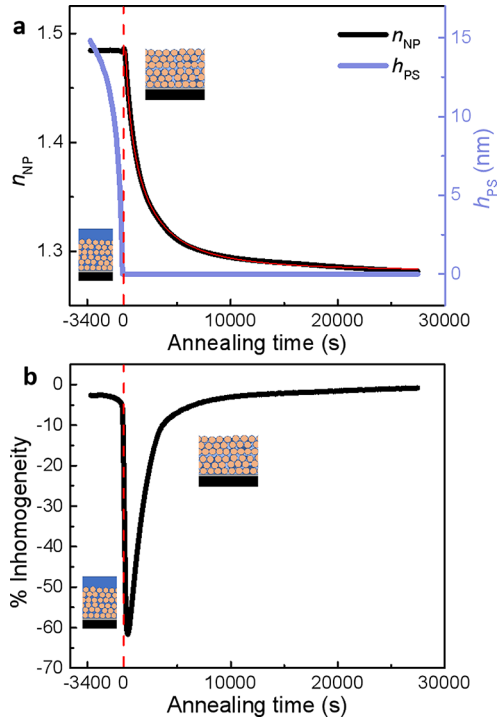

Figure 2. (a) Index of refraction of the NP layer (n_{NP}, black, left axis) and the thickness of the top PS layer (h_{PS}, blue, right axis) of a PS (8K)/SiO_2 (100 nm) film during isothermal degradation at 543 K. The degradation of PS inside the NP layer (confined PS) begins once the top PS layer is completely degraded (h_{PS} = 0, set as time t = 0 s). The red curve is an empirical stretched exponential decay fit to the data. The initial thickness of the PS and NP layers was ~15 nm and ~200 nm, respectively. The thickness of the NP layer was held constant. (b) The % inhomogeneity of the index of refraction of the NP layer during degradation.

indicating that the confined PS is not degrading during this stage. The confined PS only begins to degrade after the full degradation of the top layer. Another interesting feature of these data is the observation of inhomogeneous degradation once the degradation of the confined PS begins (Figure 2b). Using a model with linearly graded index of refraction for n_{NP}, we can see that the index inhomogeneity initially grows sharply and then decreases as the degradation proceeds. The inhomogeneity is negative, meaning that the index of refraction is lower near the free surface of the NP film (more details in the SI and Figure S1b). The delayed and inhomogeneous degradation is observed in all CaRI films with various NP diameters (11 nm < D < 100 nm). Significantly, the rate of degradation is slower as the NP size is decreased, indicating enhanced thermal stability for PS confined in smaller pores.

To gain more insight into the degradation mechanism and kinetics, the SE data at each time point were fit to a model with an exponentially graded index of refraction for the NP film. This model presents a more accurate fit to the experimental data with large inhomogeneity compared to the linearly graded model used in Figure 2 (more details in SI and Figure S2). Figure 3a shows typical results of the index of refraction as a function of the distance from the surface, in the NP layer of a PS (8K)/SiO_2 (25 nm) sample at different annealing times at 543 K. There are two steps of degradation. In the first ~600 s, the index of refraction at the film's surface drops rapidly, while it remains constant at the film's center. The film center index value starts to decrease uniformly with a much slower rate after

DOI: 10.1021/acsmacrolett.9b00649
ACS Macro Lett. 2019, 8, 1413−1418

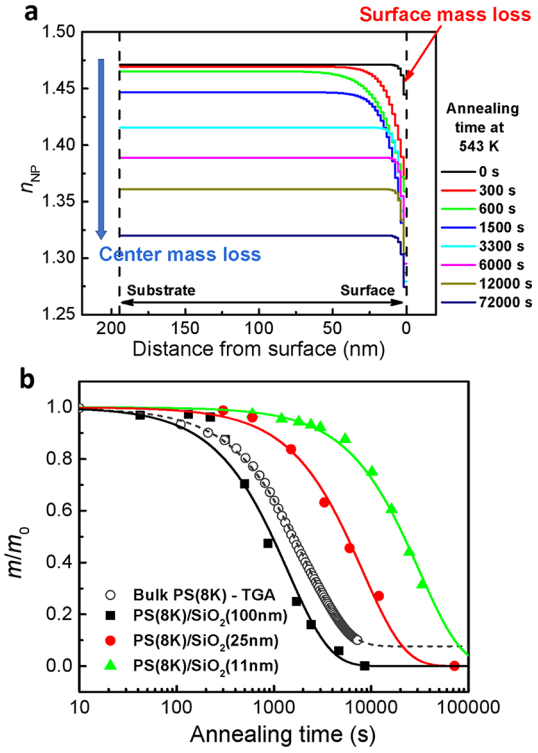

Figure 3. (a) Index of refraction as a function of distance from the substrate of the NP layer for a PS (8K)/SiO_2 (25 nm) CaRI film at various times during isothermal degradation at 543 K in ambient conditions. The NP layer thickness was ~190 nm. Time t = 0 s is defined as when the top PS layer is fully degraded as shown in Figure 2a. (b) Mass loss of PS (8K)/SiO_2 CaRI films of various NP sizes during isothermal degradation at 543 K. The gray hollow symbols show isothermal degradation of bulk PS (8K) measured by TGA. The curves show a simple exponential decay fit to the data with the corresponding color. The initial mass of the bulk (TGA) and confined (CaRI) PS is ~2 mg and ~0.01 mg, respectively.

the full degradation of the surface layer, observed as a reduction of the index gradient. The same steps are observed for degradation at various temperatures and for all NP sizes studied here (Figure S3).

Focusing first on the film center degradation process, Figure 3b shows the mass loss during isothermal degradation of three CaRI samples at 543 K in ambient conditions, along with degradation of bulk PS at the same temperature, measured using thermogravitometric analysis (TGA). Figure S10 shows the influence of sample mass on the degradation rate of TGA, indicating that a sample with comparable mass as the CaRI film would degrade even faster. These data are extracted from the index of refraction at the center of the film, i.e., the plateau value of index as shown in Figure 3a. The residual mass of both bulk and confined PS can be fitted to a simple exponential decay function ($\frac{m}{m_0} = \exp(-t/\tau) + \frac{m_{inf}}{m_0}$), where m, m_0, and m_{inf} are the mass of PS during, before, and after degradation, respectively. t is the annealing time, and τ is the characteristic degradation time. Figure 3b shows that τ is slowed by about a factor of 30 in 11 nm NPs compared to the 100 nm NPs or the bulk PS at this temperature.

Due to char formation during isothermal degradation of bulk PS in ambient conditions,[33,34] the final residual mass m_{inf} is nonzero for the bulk TGA data. m_{inf} is thus assumed to be a fitting parameter and is measured to be ~8% of the initial mass. Significantly, no charring is observed in the degradation of confined PS, even for the large NP sizes (details in SI and Figure S4). As such, m_{inf} is set to zero for the confined PS measurements. SEM images (Figure S11) and XPS (Figure S8) of CaRI films also do not show any evidence of charring. The absence of char, along with improved thermal stability, is in contrast to the previous observations in PS−clay nanocomposites, where the char formation was considered the main mechanism for improved thermal stability.[33,34]

Isothermal degradation measurements were performed at various temperatures on CaRI films with various NP layer thicknesses (120−500 nm). Figure 4a shows a plot of the

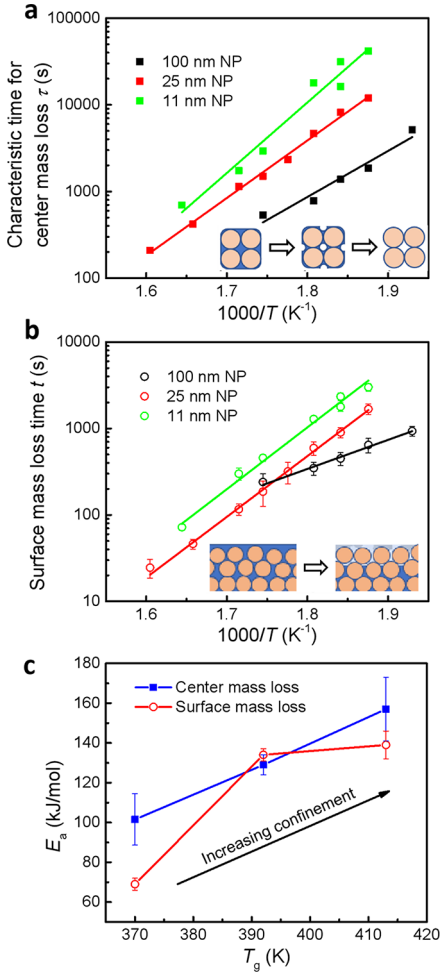

Figure 4. (a) Characteristic time for the isothermal degradation in the film center τ vs $1/T$ of PS (8K) and in CaRI films with three different NP sizes. (b) The time to reach maximum inhomogeneity during isothermal degradation t vs $1/T$, of the same CaRI films. The lines show linear fit to each data set in a and b. (c) Activation energy of the film center and surface degradation vs T_g of PS in CaRI films. The T_g data are from ref 16.

characteristic time for degradation of confined PS, $\log(\tau)$, as a function of $1/T$ for NPs of various diameters. Despite the variations in film thickness values, as long as a bulk-like layer is observed in the film, the degradation rate appears to follow an Arrhenius equation in the temperature range of our measurements. The activation energies for the degradation for the NP film center were measured based on the slopes of the Arrhenius lines to be 102 ± 13 kJ/mol, 129 ± 5 kJ/mol, and 157 ± 16 kJ/mol for PS confined in 100, 25, and 11 nm

DOI: 10.1021/acsmacrolett.9b00649
ACS Macro Lett. 2019, 8, 1413−1418

NPs, respectively (Figure 4c). These measurements show that under extreme nanoconfinement conditions the barrier for thermal degradation of the confined PS is significantly higher than the corresponding barrier for PS confined in larger NPs, as well as bulk PS, reported to be ~125 kJ/mol (M_w = 280 kg/mol).[35]

Polystyrene degrades through free radical diffusion and chain scission.[25] In the presence of O_2 in ambient conditions, the formation of highly active peroxy radicals significantly accelerates the degradation, making PS a highly flammable material.[36] Since the rate-limiting step of the thermo-oxidative degradation of PS is the bimolecular decomposition of the peroxides,[35] the slower dynamics of the confined PS can decrease the rate of this reaction. Reduced diffusion of both oxygen and the free radicals under confinement increases the thermal stability and reduces the flammability. According to our previous studies, the segmental dynamics is suppressed, and the viscosity is increased with increased degree of confinement,[9,10,16] consistent with the observation of slower degradation and higher barrier to degradation in this study. Longer lifetime of radicals and reduced termination rate during free-radical polymerization in controlled pore glass were also observed in previous studies, consistent with our observations.[19,24,37]

We have previously shown that undersaturated CaRI (UCaRI) films can be made with an insufficient amount of top PS. In UCaRI the T_g further increases due to the stronger confinement.[16,32] Figure S6 shows the characteristic degradation time at 573 K in UCaRI films with 11 nm NPs and different initial PS fill fractions. Indeed, the thermal stability is further enhanced under stronger confinement in UCaRI films, further indicating the important role of the slow down of oxygen and free radical diffusion in the enhancement of thermal stability.

In order to evaluate the thickness and the degradation rate of the surface layer, index of refraction profiles were measured on various NP sizes and film thicknesses. Figure 5a shows the profiles of the index of refraction, at the time point where the index of refraction shows the strongest inhomogeneity. The data show that for each NP size, the thickness of the surface layer, where the rate of degradation is faster than bulk, roughly corresponds to one NP diameter. This is independent of the total thickness of the NP layer, as shown in Figure S7. The faster rate of surface degradation is likely due to imperfections at the free surface of the CaRI film as well as more oxygen availability compared to the film center. As the NP diameter is decreased, the thickness of the surface layer also decreases, and its degradation slows, resulting in exceedingly increased stability in the layer as a whole because the film center degradation does not start until the surface layer is degraded (Figure 3).

Figure 4b shows the plot of the surface degradation time, the time to reach maximum inhomogeneity (Figure 2b), vs $1/T$. Unlike the film center mass loss, where the degradation is independent of the NP layer thickness, the surface degradation appears to be a layer-by layer material loss process. Thus, the total degradation time for the 100 nm NPs can be longer than that of 25 nm NPs at some temperatures, while the activation energy remains lower.

Figure 4c shows the activation energy for the degradation of the confined PS in the film center as well as the surface vs T_g.[16] It is remarkable that both the surface and film center degradation rates correlate well with the T_g increase, with

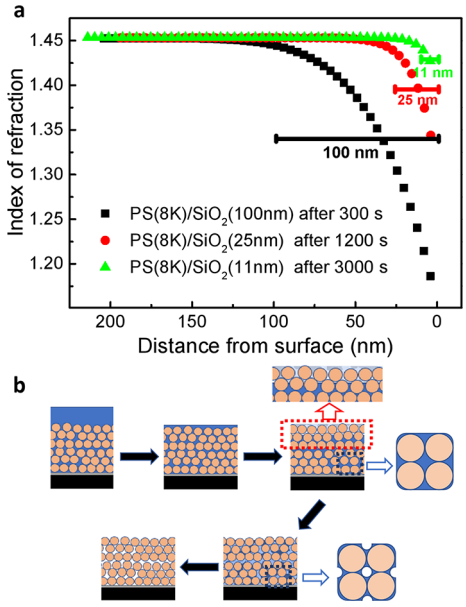

Figure 5. (a) Profile of the index of refraction at the same stage after the beginning of the film center degradation of CaRI samples with different NP sizes and film thicknesses. The scale bars represent the diameter of the NPs. The degradation temperature is 543 K. (b) Proposed mechanisms of thermal degradation in CaRI films. The hollow arrows shows the zoomed-in version of the schematics.

reasonably similar activation energies at smaller particle sizes, indicating that both processes are slowed due to the slow down of the kinetics of the confined PS itself. The slower characteristic time of degradation in the NP film center compared to the surface likely stems from slower oxygen diffusion toward the center of the film as well as the slower diffusion of the products. Combined, these data indicate that the degradation process in these highly confined systems is diffusion limited and proceeds through free surfaces.

Based on the data shown in Figure 4, we propose a two-step diffusion-limited degradation in CaRI films, schematically sketched in Figure 5b. After the full degradation of the top PS layer, i.e., the beginning of the degradation of confined PS, the PS at the surface layer of NPs, which has better access to oxygen, degrades first. The products of the reaction for this layer can readily diffuse out of the layer, with a rate that is dependent on the viscosity of the layer and thus correlates with T_g.

After the removal of the first layer, the film essentially becomes an underfilled (UCaRI) layer, where there is a gradient of mobility in the dynamics. The material at the center of the larger pores has lower viscosity and higher diffusion and, thus, degrades first, while the remaining PS moves toward smaller pores and becomes more confined, as previously reported in UCaRI systems.[16] In UCaRI films, the spatial confinement has a stronger effect on the dynamics of the confined PS increasing T_g and thus its effective viscosity.[16] As shown in Figure S6, this also results in slower rate of degradation in UCaRI films. As such, it is reasonable to assume that the material in the center of the pores degrades first, slowly removing products as the degradation continues toward the NP surfaces.

To verify this hypothesis, SEM images were obtained of a PS (8K)/SiO_2 (25 nm) sample where ~40% of the PS in the film center is degraded. From the cross-section SEM image (Figure

DOI: 10.1021/acsmacrolett.9b00649
ACS Macro Lett. 2019, 8, 1413−1418

S5a), it is observed that the sample contains large pores, and the PS is uniformly distributed throughout the film, as expected. Moreover, no PS is seen in the first layer from the top-view image (Figure S5b), indicating the complete degradation of the surface layer. These observations indicate that even in the film's center the degradation is through the free surface and proceeds toward the NP surfaces, meaning that the availability of oxygen and product diffusion are rate-limiting steps even in the film center.

The diffusion-limited degradation process, even in relatively large 100 nm NP particles, means that the process is distinctly different than bulk PS degradation, despite the fact that the activation energy of degradation in 100 nm NPs is reasonably similar to that of bulk PS. This difference has important consequences in the molecular weight distribution of the products as well as the flammability of PS in CaRI films. Since diffusion is strongly dependent on the size of the reaction products, it is expected that the smaller products would diffuse out of the film faster, allowing time for the larger products to break apart. As such, we hypothesize that the distribution of the molecular weight in CaRI films will be weighted toward smaller products such as styrene and toluene. This will be explored in our future work.

Remarkably, the cross-linking of the reaction products that results in char formation as well as the autoacceleration of the degradation reaction and therefore PS flammability also slow down in CaRI. This is because the degradation is primarily occurring at the free PS surfaces even in the film center. As such, unlike the bulk PS, the degradation in CaRI proceeds until all the material is removed without leaving any noticeable residual layer or char (Figures S4 and S8 and more discussion in the SI). This suppression of char formation is potentially of interest in developing flame-retardant coatings using flammable polymers, by producing highly confined states.

These observations are in sharp contrast with the degradation of PS in the PNC systems reported previously, where the thermal stability of PS/SiO_2 nanocomposites is not as significant as PS/clay nanocomposites.[26,28] In our study, the degradation rate at 573 K of PS in 11 nm NP packings is significantly slower than the rate at 543 K in 100 nm NPs or bulk PS. To our knowledge, this is the highest reported degree of improvement of the thermal stability of PS/SiO_2 composite systems. In CaRI systems without significant interaction between the NPs and PS, we have previously demonstrated that entropic effects result in increased viscosity[9,10] and T_g,[16] which are in turn promoting enhanced thermal stability here. The enhanced thermal stability is also observed for PS well above the entanglement molecular weight (Figure S9). It remains to be explored how NP/polymer interactions and molecular weight in extreme confinement would affect these observations.

In summary, we studied the thermal degradation of PS under extreme nanoconfinement using CaRI as a model system. The degree of confinement is controlled using SiO_2 NPs with diameters ranging from 11 to 100 nm, resulting in the pore diameters ranging from ∼3 nm to ∼30 nm. We show that in this weakly interacting system strong spatial confinement results in unprecedented enhancement of the thermal stability of PS in ambient conditions. In isothermal degradation experiments both the characteristic time of degradation and the activation energy for degradation increase, with values that correlate with increased T_g in these systems. The details of degradation indicate that the degradation proceeds through surfaces and from the center of larger holes toward NP surfaces, reducing the flammability and the ability of the system to form char. These observations indicate that even in relatively large pores for the 100 nm NPs the process of degradation is diffusion limited and is stabilized due to the slower diffusion of the free radicals, oxygen, and the reaction products.

■ ASSOCIATED CONTENT

Supporting Information

The Supporting Information is available free of charge on the ACS Publications website at DOI: 10.1021/acsmacrolett.9b00649.

Detailed sample preparation; ellipsometry measurements and modeling; TGA characterization; SEM during thermal degradation; UCaRI; XPS; and high Mw PS degradation (PDF)

■ AUTHOR INFORMATION

Corresponding Author

*E-mail: fakhraai@sas.upenn.edu.

ORCID

Haonan Wang: 0000-0003-2047-5380
Kevin T. Turner: 0000-0003-4963-4568
Daeyeon Lee: 0000-0001-6679-290X
Zahra Fakhraai: 0000-0002-0597-9882

Author Contributions

H.W, P.M., D.L., and Z.F. designed research; H.W., A.A.S, and Y.Q. performed research; H.W., A.A.S, and Z.F. analyzed data; and H.W. and Z.F. wrote the paper.

Notes

The authors declare no competing financial interest.

■ ACKNOWLEDGMENTS

This research was primarily supported by the National Science Foundation (NSF) through the University of Pennsylvania Materials Research Science and Engineering Center (MRSEC) (DMR-1720530) and partially by the NSF-1662695 grant and Corning Research and Development Corporation (CRDC) (H.W.). MRSEC facilities were used for TGA and SEM imaging (NSF DMR-1720530). We thank Professor Baumgart's lab for the plasma cleaner and Steven Szewczyk for the TGA. We thank Professor Masoud Soroush and Drexel Centralized Research Facilities (CRF) for the XPS instruments.

■ REFERENCES

(1) Ediger, M. D.; Forrest, J. A. Dynamics near Free Surfaces and the Glass Transition in Thin Polymer Films: A View to the Future. *Macromolecules* **2014**, *47*, 471−478.
(2) Fakhraai, Z.; Forrest, J. A. Measuring the Surface Dynamics of Glassy Polymers. *Science* **2008**, *319*, 600−604.
(3) Huang, Y.; Paul, D. R. Physical Aging of Thin Glassy Polymer Films Monitored by Optical Properties. *Macromolecules* **2006**, *39*, 1554−1559.
(4) Priestley, R. D. Structural Relaxation of Polymer Glasses at Surfaces, Interfaces, and In Between. *Science* **2005**, *309*, 456−459.
(5) Pye, J. E.; Rohald, K. A.; Baker, E. A.; Roth, C. B. Physical Aging in Ultrathin Polystyrene Films: Evidence of a Gradient in Dynamics at the Free Surface and Its Connection to the Glass Transition Temperature Reductions. *Macromolecules* **2010**, *43*, 8296−8303.

DOI: 10.1021/acsmacrolett.9b00649
ACS Macro Lett. 2019, 8, 1413−1418

(6) Baker, E. A.; Rittigstein, P.; Torkelson, J. M.; Roth, C. B. Streamlined Ellipsometry Procedure for Characterizing Physical Aging Rates of Thin Polymer Films. *J. Polym. Sci., Part B: Polym. Phys.* **2009**, *47*, 2509−2519.
(7) Pye, J. E.; Roth, C. B. Above, Below, and In-between the Two Glass Transitions of Ultrathin Free-standing Polystyrene Films: Thermal Expansion Coefficient and Physical Aging. *J. Polym. Sci., Part B: Polym. Phys.* **2015**, *53*, 64−75.
(8) Bodiguel, H.; Fretigny, C. Reduced Viscosity in Thin Polymer Films. *Phys. Rev. Lett.* **2006**, *97*, 266105.
(9) Hor, J. L.; Wang, H.; Fakhraai, Z.; Lee, D. Effect of Polymer-nanoparticle Interactions on the Viscosity of Unentangled Polymers under Extreme Nanoconfinement during Capillary Rise Infiltration. *Soft Matter* **2018**, *14*, 2438−2446.
(10) Hor, J. L.; Wang, H.; Fakhraai, Z.; Lee, D. Effect of Physical Nanoconfinement on the Viscosity of Unentangled Polymers during Capillary Rise Infiltration. *Macromolecules* **2018**, *51*, 5069−5078.
(11) Forrest, J. A.; Mattsson, J. Reductions of the Glass Transition Temperature in Thin Polymer Films: Probing the Length Scale of Cooperative Dynamics. *Phys. Rev. E: Stat. Phys., Plasmas, Fluids, Relat. Interdiscip. Top.* **2000**, *61*, R53−R56.
(12) Keddie, J. L.; Jones, R. A. L.; Cory, R. A. Size-Dependent Depression of the Glass Transition Temperature in Polymer Films. *Europhysics Letters (EPL)* **1994**, *27*, 59−64.
(13) Batistakis, C.; Lyulin, A. V.; Michels, M. A. J. Slowing Down versus Acceleration in the Dynamics of Confined Polymer Films. *Macromolecules* **2012**, *45*, 7282−7292.
(14) Rittigstein, P.; Priestley, R. D.; Broadbelt, L. J.; Torkelson, J. M. Model Polymer Nanocomposites Provide an Understanding of Confinement Effects in Real Nanocomposites. *Nat. Mater.* **2007**, *6*, 278−282.
(15) Glor, E. C.; Fakhraai, Z. Facilitation of Interfacial Dynamics in Entangled Polymer Films. *J. Chem. Phys.* **2014**, *141*, 194505.
(16) Wang, H.; Hor, J. L.; Zhang, Y.; Liu, T.; Lee, D.; Fakhraai, Z. Dramatic Increase in Polymer Glass Transition Temperature under Extreme Nanoconfinement in Weakly Interacting Nanoparticle Films. *ACS Nano* **2018**, *12*, 5580−5587.
(17) Zhao, H.; Sen, S.; Udayabhaskararao, T.; Sawczyk, M.; Kučanda, K.; Manna, D.; Kundu, P. K.; Lee, J.-W.; Král, P.; Klajn, R. Reversible Trapping and Reaction Acceleration within Dynamically Self-assembling Nanoflasks. *Nat. Nanotechnol.* **2016**, *11*, 82−88.
(18) Li, J.; Wei, Y.; Chen, J.; Xu, S.; Tian, P.; Yang, X.; Li, B.; Wang, J.; Liu, Z. Cavity Controls the Selectivity: Insights of Confinement Effects on MTO Reaction. *ACS Catal.* **2015**, *5*, 661−665.
(19) Zhao, H.; Simon, S. L. Methyl Methacrylate Polymerization in Nanoporous Confinement. *Polymer* **2011**, *52*, 4093−4098.
(20) Begum, F.; Simon, S. L. Modeling Methyl Methacrylate Free Radical Polymerization in Nanoporous Confinement. *Polymer* **2011**, *52*, 1539−1545.
(21) Lopez, E.; Simon, S. L. Trimerization Reaction Kinetics and Tg Depression of Polycyanurate under Nanoconfinement. *Macromolecules* **2015**, *48*, 4692−4701.
(22) Zhao, H.; Simon, S. L. Equilibrium Free-radical Polymerization of Methyl Methacrylate under Nanoconfinement. *Polymer* **2015**, *66*, 173−178.
(23) Zhao, H.; Yu, Z.; Begum, F.; Hedden, R. C.; Simon, S. L. The Effect of Nanoconfinement on Methyl Methacrylate Polymerization: T G, Molecular Weight, and Tacticity. *Polymer* **2014**, *55*, 4959−4965.
(24) Uemura, T.; Ono, Y.; Kitagawa, K.; Kitagawa, S. Radical Polymerization of Vinyl Monomers in Porous Coordination Polymers: Nanochannel Size Effects on Reactivity, Molecular Weight, and Stereostructure. *Macromolecules* **2008**, *41*, 87−94.
(25) Chrissafis, K.; Bikiaris, D. Can Nanoparticles Really Enhance Thermal Stability of Polymers? Part I: An Overview on Thermal Decomposition of Addition Polymers. *Thermochim. Acta* **2011**, *523*, 1−24.
(26) Bera, O.; Pilić, B.; Pavličević, J.; Jovičić, M.; Holló, B.; Szécsényi, K. M.; Špirkova, M. Preparation and Thermal Properties of Polystyrene/silica Nanocomposites. *Thermochim. Acta* **2011**, *515*, 1−5.
(27) Bourbigot, S.; Gilman, J. W.; Wilkie, C. A. Kinetic Analysis of the Thermal Degradation of Polystyrene−montmorillonite Nanocomposite. *Polym. Degrad. Stab.* **2004**, *84*, 483−492.
(28) Vaziri, H. S.; Omaraei, I. A.; Abadyan, M.; Mortezaei, M.; Yousefi, N. Thermophysical and Rheological Behavior of Polystyrene/silica Nanocomposites: Investigation of Nanoparticle Content. *Mater. Eng.* **2011**, *32*, 4537−4542.
(29) Li, H.; Yu, Y.; Yang, Y. Synthesis of Exfoliated Polystyrene/montmorillonite Nanocomposite by Emulsion Polymerization Using a Zwitterion As the Clay Modifier. *Eur. Polym. J.* **2005**, *41*, 2016−2022.
(30) Awad, W. H. High-Throughput Method for the Synthesis of High Performance Polystyrene Nanocomposites. *Polym.-Plast. Technol. Eng.* **2006**, *45*, 1117−1122.
(31) Huang, Y.-R.; Jiang, Y.; Hor, J. L.; Gupta, R.; Zhang, L.; Stebe, K. J.; Feng, G.; Turner, K. T.; Lee, D. Polymer Nanocomposite Films with Extremely High Nanoparticle Loadings Via Capillary Rise Infiltration (CaRI). *Nanoscale* **2015**, *7*, 798−805.
(32) Hor, J. L.; Jiang, Y.; Ring, D. J.; Riggleman, R. A.; Turner, K. T.; Lee, D. Nanoporous Polymer-Infiltrated Nanoparticle Films with Uniform or Graded Porosity via Undersaturated Capillary Rise Infiltration. *ACS Nano* **2017**, *11*, 3229−3236.
(33) Kumar, A. P.; Depan, D.; Tomer, N. S.; Singh, R. P. Nanoscale Particles for Polymer Degradation and Stabilization—trends and Future Perspectives. *Prog. Polym. Sci.* **2009**, *34*, 479−515.
(34) Gilman, J. W.; Harris, R. H.; Shields, J. R.; Kashiwagi, T.; Morgan, A. B. A Study of the Flammability Reduction Mechanism of Polystyrene-layered Silicate Nanocomposite: Layered Silicate Reinforced Carbonaceous Char. *Polym. Adv. Technol.* **2006**, *17*, 263−271.
(35) Peterson, J. D.; Vyazovkin, S.; Wight, C. A. Kinetics of the Thermal and Thermo-Oxidative Degradation of Polystyrene, Polyethylene and Poly(propylene). *Macromol. Chem. Phys.* **2001**, *202*, 775−784.
(36) Vyazovkin, S.; Dranca, I.; Fan, X.; Advincula, R. Kinetics of the Thermal and Thermo-Oxidative Degradation of a Polystyrene−Clay Nanocomposite. *Macromol. Rapid Commun.* **2004**, *25*, 498−503.
(37) Ng, S. M.; ichi Ogino, S.; Aida, T.; Koyano, K. A.; Tatsumi, T. Free Radical Polymerization within Mesoporous Zeolite Channels. *Macromol. Rapid Commun.* **1997**, *18*, 991−996.

DOI: 10.1021/acsmacrolett.9b00649
ACS Macro Lett. 2019, 8, 1413−1418